UC San Diego

UC San Diego Previously Published Works

Title

Graphene Nanopore Support System for Simultaneous High-Resolution AFM Imaging and Conductance Measurements

Permalink

https://escholarship.org/uc/item/8wr343p8

Journal

ACS Applied Materials & Interfaces, 6(7)

ISSN

1944-8244

Authors

Connelly, Laura S
Meckes, Brian
Larkin, Joseph
et al.

Publication Date

2014-04-09

DOI

10.1021/am500639q

Peer reviewed

eScholarship.org Powered by the California Digital Library
University of California

This is an open access article published under an ACS AuthorChoice License, which permits copying and redistribution of the article or any adaptations for non-commercial purposes.

ACS APPLIED MATERIALS & INTERFACES

Research Article

www.acsami.org

Graphene Nanopore Support System for Simultaneous High-Resolution AFM Imaging and Conductance Measurements

Laura S. Connelly,[†,§,⊥] Brian Meckes,[‡,⊥] Joseph Larkin,[∥] Alan L. Gillman,[‡] Meni Wanunu,[∥] and Ratnesh Lal*[,†,‡,§]

[†]Materials Science and Engineering Program, [‡]Department of Bioengineering, and [§]Department of Mechanical and Aerospace Engineering, University of California—San Diego, 9500 Gilman Drive, La Jolla, California 92093, United States

[∥]Department of Physics, Northeastern University, 110 Forsyth Street, Boston, Massachusetts 02115, United States

ABSTRACT: Accurately defining the nanoporous structure and sensing the ionic flow across nanoscale pores in thin films and membranes has a wide range of applications, including characterization of biological ion channels and receptors, DNA sequencing, molecule separation by nanoparticle films, sensing by block co-polymers films, and catalysis through metal—organic frameworks. Ionic conductance through nanopores is often regulated by their 3D structures, a relationship that can be accurately determined only by their simultaneous measurements. However, defining their structure—function relationships directly by any existing techniques is still not possible. Atomic force microscopy (AFM) can image the structures of these pores at high resolution in an aqueous environment, and electrophysiological techniques can measure ion flow through individual nanoscale pores. Combining these techniques is limited by the lack of nanoscale interfaces. We have designed a graphene-based single-nanopore support (~5 nm thick with ~20 nm pore diameter) and have integrated AFM imaging and ionic conductance recording using our newly designed double-chamber recording system to study an overlaid thin film. The functionality of this integrated system is demonstrated by electrical recording (<10 pS conductance) of suspended lipid bilayers spanning a nanopore and simultaneous AFM imaging of the bilayer.

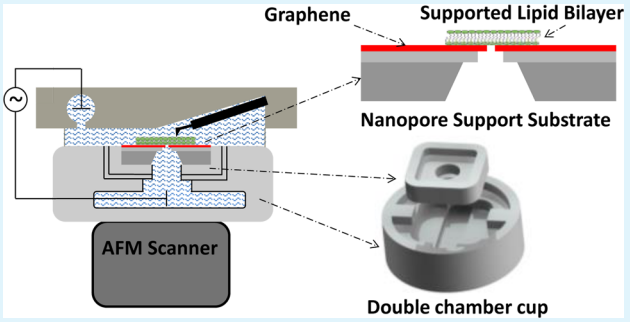

KEYWORDS: *atomic force microscopy, solid-state nanopore, electrophysiology, microscopy, suspended lipid bilayers, ionic conductance*

INTRODUCTION

In recent years, advancement in fabrication techniques has led to novel nanoporous structures with an array of applications in biotechnology,[1−5] polymer science,[6] and energy.[7,8] Small changes in the nanoscale features of these pores determine the specific conducting properties of ions through and around the pores.[9−11] Ion-conducting nanopores, including biological channels and receptors, may also interact with the surrounding environment and change over time. For example, living systems rely on the coordinated activity of membrane ion channels and receptors that control ionic and metabolic homeostasis and cell—cell/extracellular communications through regulation of ions, metabolites, and RNA transport. Dysfunction of ion channels is associated with pathophysiology and diseases such as Alzheimer's disease and Parkinson's disease, addiction, and some genetic disorders.[12−15] Improved therapeutic development, diagnosis, and/or prevention is therefore dependent on an accurate understanding of these channels' structure—activity relationship.

To fully understand the structure—function relationship of nanopore-containing thin films and membranes, structure and function must be correlated directly through simultaneous measurements. However, current techniques cannot provide real-time, direct, and simultaneous observation of the 3D structure and activity of these pores.

Atomic force microscopy (AFM) allows dynamic high-resolution imaging of biological samples in physiological environments,[16−22] including 3D structures of individual ion channels in native hydrated environments.[12,13,16,23−30] The open interface of the AFM allows its integration with other techniques, including bilayer electrical recording and light/fluorescence microscopy. The missing link for integrating AFM imaging and electrical recording is a lack of an appropriate nanoscale support system.

Nanopore samples have emerged as an exciting class of nanosensors that have gained attention for their sensitivity to conductance changes, especially in relation to the translocation of biomolecules, and numerous nanoporous devices have been made from natural, artificial, and hybrid materials.[1,3−5,31−38] Graphene is a promising and reliable material because of its unique mechanical, electronic, thermal, and optical properties.[31,34,35,39−41] Graphene is thin enough to be precisely drilled using a transmission electron microscope (TEM) and is strong

Received: January 28, 2014
Accepted: February 28, 2014
Published: February 28, 2014

 © 2014 American Chemical Society

enough to be freely suspended over microscale pores.[10,31,35,42,43] Although much of the recent research on single-nanopore conductance has been directed toward the application of DNA sequencing or biomolecule translocation, micro- and nanopore devices have also been used to study the activity of ion channels.[15,44]

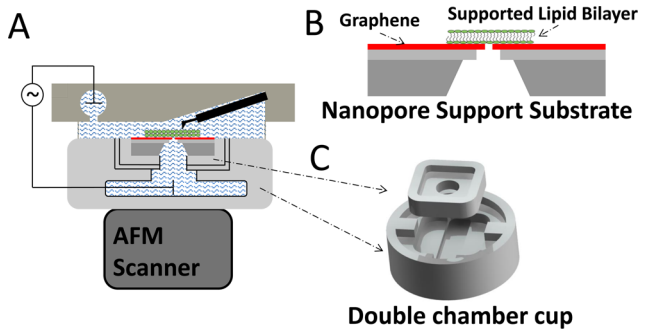

Figure 1. Schematic of the integrated AFM system for imaging and conductance measurements. (A) The nanopore support is glued into the top chamber of the double-chamber cup such that the only liquid path connecting the chambers is through the deposited lipid bilayer (green) over the nanopore. The double-chamber cup is placed on the scanner head, and the liquid cell with mounted cantilever is placed on top of the sample to allow for AFM imaging. Electrodes are connected to the bottom chamber though the double-chamber cup and to the top solution through an open port in the liquid cell for measuring conductance activity. The electrodes are fed to an amplifier and computer for analysis. (B) Schematic of the nanopore support (black) with a deposited lipid bilayer (green) suspended over the pore to seal the ionic conductance. (C) Schematic image of the double-chamber cup design. The nanopore support from panel B fits into the top removable piece and is set into the bottom piece.

Here, we describe a novel graphene nanopore support system (Figure 1) for simultaneous localized high-resolution AFM and ionic conductance recording of nanoporous thin films. Solid-state single-nanopore support substrates were fabricated to fit into the open interface of the multimode AFM with our recently developed two-chamber system (Figure 1). We demonstrate the applicability of the integrated nanopore support system combining AFM imaging and electrical recording using suspended lipid bilayers. We show that a lipid bilayer deposited over the graphene nanopore seals the pore. These bilayers can be imaged repeatedly with AFM and retain their electrical properties. Electrical conductance measurements reveal a dramatic reduction in the conductance, >1 μS for the open pore to <10 pS, for the bilayer-covered pores, indicating complete coverage and sealing of the nanopore. The device and setup that we present here demonstrates the imaging resolution, nanopore size, and conductance sensitivity on scales compatible with what is needed for the structure–activity study of ion channels. The use of this technology would have major implications for, but not limited to, the study of neurological disorders, pathological studies, therapeutic screening, and drug addiction.

MATERIALS AND METHODS

Materials. Silicon oxide membranes (SiO_2) were purchased from AppNano (Mountain View, CA). Silicon oxide membranes are 200 nm thick and 20 × 20 μm^2 wide freestanding windows supported by a 300 μm thick silicon substrate. The windows were formed by KOH anisotropic etching of a 450 × 450 μm^2 opening on the backside of the silicon support (Figures 2A and 3A). Single-layer CVD graphene deposited on 20 μm thick Cu foil (2 × 2″) was obtained from Graphene Supermarket (Calverton, NY). A Quanta 3D FEG focused ion beam (FIB) was used to drill through the SiO_2 suspended membrane. Either an iron(III) chloride hexahydrate ($FeCl_3 \cdot 6H_2O$; ≥

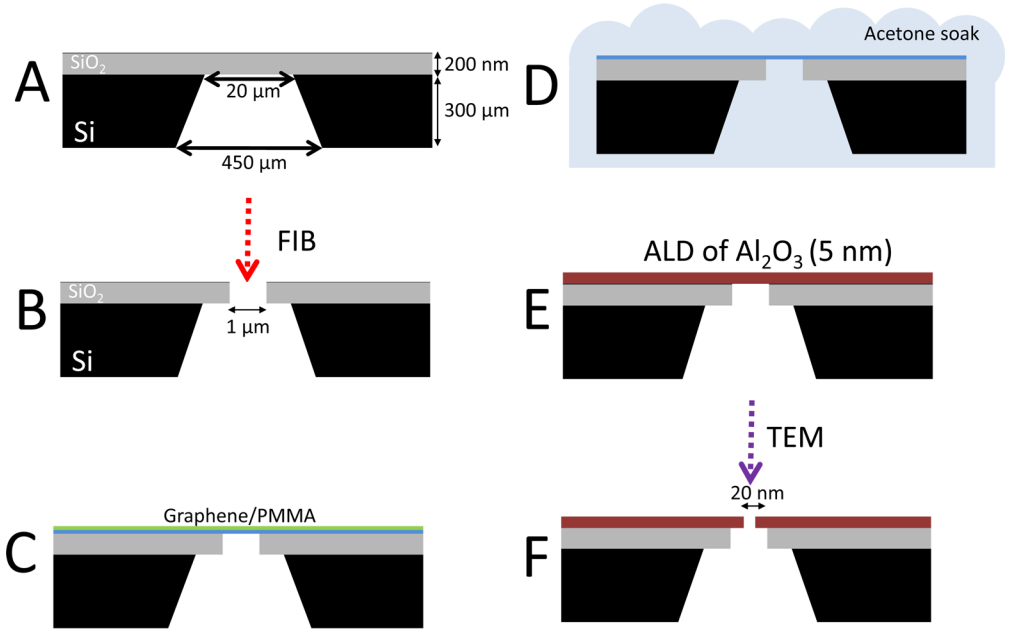

Figure 2. Cross-sectional schematic sequencing of the processing of a solid-state substrate containing a single nanopore. (A) The starting substrate is a 6 mm × 6 mm × 300 μm silicon substrate (black) with a 200 nm SiO_2 layer (gray). A 20 × 20 μm^2 window of suspended SiO_2 is in the center of the substrate. (B) A focused ion beam (red) is used to find the center of the 20 × 20 μm^2 SiO_2 window and to drill a 1 μm hole. (C) A graphene flake (blue) coated with PMMA (green) floating on the surface of H_2O is placed over the 1 μm FIB hole and allowed to dry. (D) Acetone is used to dissolve the PMMA, leaving a graphene sheet suspended over the 1 μm hole. (E) Five nanometers of Al_2O_3 (red) is deposited by atomic layer deposition (ALD) over the graphene. (F) TEM (purple) is used to drill a single nanopore in the center of the 1 μm hole.

dx.doi.org/10.1021/am500639q | ACS Appl. Mater. Interfaces 2014, 6, 5290–5296

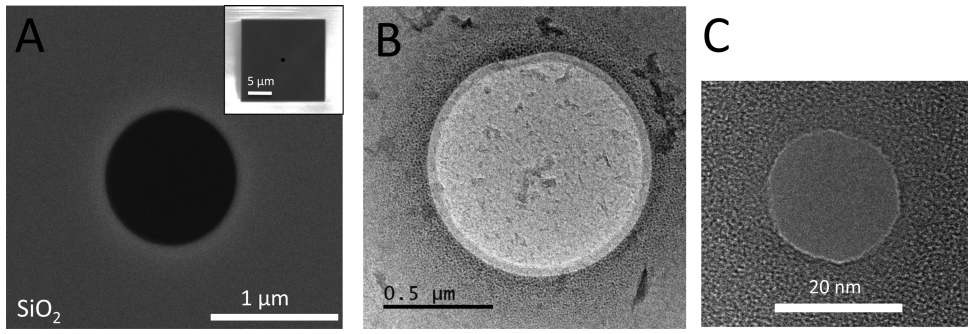

Figure 3. (A) Top-view SEM image of the drilled FIB 1 μm hole. Inset is a zoomed-out SEM image of the same hole. The 20 × 20 μm^2 SiO_2 window is visible in the SEM image. Scale bar = 1 μm. (B) TEM image of the drilled FIB 1 μm hole covered with a layer of graphene showing no defects. Thicker regions appear darker. Scale bar = 500 nm. (C) TEM image of a single drilled 20 nm pore in the graphene/Al_2O_3 membrane. Scale bar = 20 nm.

98%) solution (Sigma Aldrich) or Copper Etch APS-100 (Transene Co.) was used to dissolve the Cu substrate of the graphene. Atomic layer deposition (ALD) of 5 nm of Al_2O_3 was performed using a GEMSTAR benchtop atomic layer deposition (ALD) process system or the Beneq TFS200 atomic layer deposition system. A transmission electron microscope (TEM) (JEOL 2010FEG, Japan) operating in bright-field imaging mode was used for drilling through the graphene/Al_2O_3 membrane layer. AFM imaging was completed using a multimode Nanoscope IV system and liquid cell (both from Bruker, Santa Barbara, CA) with silicon nitride cantilevers (k = 0.08 N/m, Asylum Research, Santa Barbara, CA). Conductance measurements were completed using a custom-designed Lexan polycarbonate double-chamber cup (Figure 1C) and Ag/AgCl wire electrodes. Ecoflex Supersoft 5 silicone-cured rubber was used as an insulating sealant of the nanopore sample in the double-chamber cup. A patch-clamp amplifier (Dagan, Minneapolis, MN) was used for amplifying currents. Electrolyte solutions at pH 8.5 containing 1 M KCl buffered with 10 mM Tris, similar to Venkatesan et al., was used for AFM imaging in liquid and conductance measurements.[45] The phospholipid 1,2-diphytanoyl-*sn*-glycero-3-phosphocholine (DiPhyPC) was purchased from Avanti Polar Lipids (Alabaster, AL).

Nanopore Fabrication Process. To fabricate a single nanopore support, the Si/SiO_2 substrates were used as a base for the processing (Figure 2A). A single hole with a diameter of 1 μm was drilled by FIB through the center of the SiO_2 20 × 20 μm^2 suspended membrane area (Figures 2B and 3A). A sample of graphene on Cu was spin-coated with PMMA for 50 s and baked at 180 °C for 10 min. The Cu foil was completely dissolved in a $FeCl_3 \cdot 6H_2O$ solution or copper etchant APS-100 (~24 h). The remaining PMMA/graphene flake was deposited over the center of the cleaned SiO_2 membranes to ensure coverage of the entire 1 μm FIB hole area and was allowed to dry (Figure 2C). Dried samples were soaked in acetone to dissolve the top layer of PMMA (Figure 2D). Five nanometers of Al_2O_3 was deposited on the sample by ALD (Figures 2E and 3B). A nanopore was then drilled through the center of the graphene/Al_2O_3-suspended membrane by TEM (Figures 2F and 3C).[1,46] The nanopore sample was cleaned with acetone, isopropanol, and UV/ozone cleaner for 15 min before use in conductance measurements.

Experimental Setup for Imaging and Conductance. The double-chamber cup was used to hold the nanopore support as previously described in Meckes et al. (Figure 1C).[47] The nanopore sample (Figure 1B) sits on the square inset of the top chamber piece and is sealed into the top chamber using a continuous layer of fast curing Ecoflex Supersoft 5 (Figure 1C).

AFM imaging in liquid was performed with deflection feedback on the nanopore sample in the double-chamber cup. An Ag/AgCl electrode was placed through a port of the liquid cell, and another similar electrode was embedded in the opposite chamber of the double-chamber cup (Figure 1A). The entire AFM base was placed in a Faraday cage on in-house bungee cord-suspended platform for noise isolation. A complete schematic of the experimental setup is shown in Figure 1A.

Lipid Bilayer Preparation. DiPhyPC liposomes were formed by drying lipids dissolved in chloroform in a rotovap. The dried lipids were hydrated with molecular grade H_2O and vortexed. The solutions were then sonicated for 10 min.

Nanopore surfaces were pretreated with a droplet of lipid−hexane solution containing 70 μL of lipid (5 mg/mL) mixed with 100 μL of hexane. Liposomes were deposited over the nanopore and incubated for 2 h at room temperature. Several drops of 1 M KCl, 10 mM Tris, 5 mM $CaCl_2$, pH 8.0, buffer were added to the incubated liposome droplet and incubated for an additional 10 min to transition single-vesicle layers to suspended single planar bilayers across the nanopore.[10] Excess Ca^{2+} and liposomes were rinsed with 1 M KCl electrolyte solution buffered with 10 mM Tris to pH 8.5. The double-chamber cup was set on the scanner head of the AFM. The area containing the nanopore, a 20 × 20 μm^2 area of 200 nm thick SiO_2, was aligned under the cantilever tip in an optical system.

Simultaneous AFM Imaging of Bilayer and Electrical Recording. Conductance levels and capacitance of the bilayers were recorded using a National Instruments DAC with a custom LabView 8.0 program and the patch-clamp amplifier under applied voltages of ±100 mV. When sufficient sealing of the nanopore was established, the AFM was engaged and, in contact mode, the area of the nanopore covered with bilayers was imaged while simultaneously recording conductance levels. Capacitance measurements were performed by feeding ramp function signals (10 mV amplitude, 10 Hz) across the bilayer. The capacitance of the membrane is proportional to the amplitude of the resulting square wave. All electrical measurements were analyzed with Clampfit 10.2. A digital lowpass Gaussian filter with a 50 Hz cutoff was applied to all data represented. Extraneous 60 Hz noise was eliminated with a digital notch filter centered at 60 Hz with a 9 Hz bandwidth.

RESULTS

AFM Analysis and Conductance Characterization of Nanopore. Images of the nanopore support were taken periodically throughout the fabrication process by electron microscopy (EM) and AFM. A 20 × 20 μm^2 suspended SiO_2 area was visible in SEM (Figure 3A inset) and in AFM (Figure 4A), enabling for the eventual centered drilling of the nanopore. The AFM height images show a large deformation pattern of the suspended SiO_2 square that is not seen in SEM (Figure 4A). This deformation is due to stress relief following the etching of the underlying Si layer. The center area of this square where the graphene membrane resides appears to have very little deformation in comparison to the edges, sufficient for imaging bilayers. The focused ion beam (FIB)-drilled hole placed in the center of this square is also visible in SEM (Figure

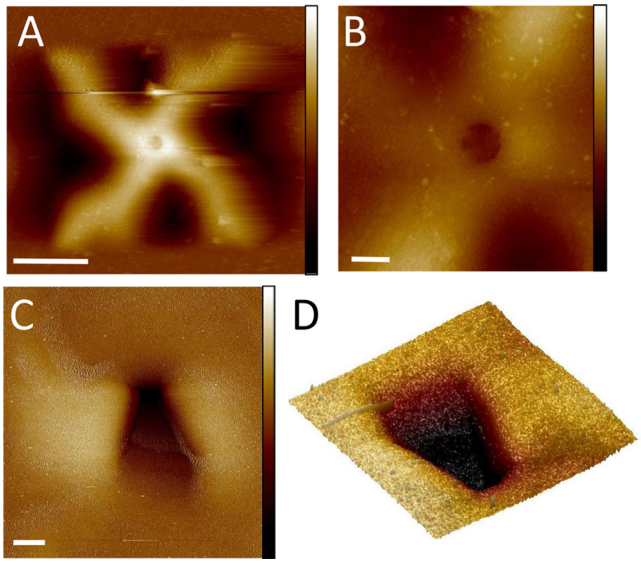

Figure 4. Progressive AFM height images in tapping mode of a complete nanopore support. (A) Image showing the complete 20 × 20 μm^2 SiO_2 area with an X-shaped deformation resulting from stress relief following the etching of the underlying Si layer. The center of the X, where the graphene membrane resides and AFM imaging will occur, shows very little localized deformation. Scale bar = 5 μm, height color scale = 294 nm. (B) Image of the FIB hole showing uniform coverage by graphene/Al_2O_3. Scale bar = 1 μm, height color scale = 208 nm. (C) Image of a single nanopore drilled in graphene/Al_2O_3. The rectangular shape of the nanopore is an effect of the shape of the tip and imaging into the pore area. Scale bar = 20 nm, height color scale = 17.8 nm. (D) Three-dimensional view of the nanopore shown in panel C. Image size is 125 × 122 nm^2.

3A), TEM (Figure 3B), and AFM even after deposition of the graphene/Al_2O_3 layer (Figure 4A,B). Complete coverage of the FIB hole with graphene was confirmed in the TEM (Figure 3B) before nanopore drilling (Figure 3C). AFM imaging reveals the nanopore (Figure 4C), which is found by sequentially zooming in on the center of the FIB hole, such as that seen in Figure 4. With a very sharp AFM tip, the nanopore size can be approximated from the AFM image and compared to the size observed in TEM (Figures 3D, 4C,D, and 6). The square shape of the nanopore shown in Figure 4C is likely due to geometry effects of the AFM tip (radius ~30 nm) and the depth of the pore.

Ion conductance measurements are a good way to probe the pore geometry.[10,11,31,37,40] Neglecting access resistance for our large pores, pore conductance relates to geometry via the following equation:[11,37]

$$G = \frac{\pi d_{pore}^2}{4L_{pore}}\left((\mu_K + \mu_{Cl})n_{KCl}e + \mu_K \frac{4\sigma}{d_{pore}}\right)$$

Where G is conductance, d_{pore} is the pore diameter, L_{pore} is the pore cylindrical length, n_{KCl} is the concentration of the buffer, e is elementary charge, σ is the surface charge density in the nanopore, and μ_K and μ_{Cl} are the electrophoretic mobilities of the two solution ions potassium and chloride. A 1 M KCl buffer was used in the work reported here. The electrophoretic mobilities of potassium and chloride are $\mu_K = 7.616 \times 10^{-8}$ $m^2/(V\ s)$ and $\mu_{Cl} = 7.909 \times 10^{-8}$ $m^2/(V\ s)$ at room temperature.[10,37]

The predicted conductance from the given equation is dependent on pore morphology and surface charge density of the sample. High surface charge density for graphene/Al_2O_3 layers is considered 200 mC/m^2, and minimum surface charge is 0 mC/m^2.[10,37] A range of solid-state nanopores was fabricated with d_{pore} values of 20−50 nm and $L_{pore} \approx 5$ nm. The expected conductance values in this nanopore size range for high and low surface charge density samples would be approximately 1100−6100 and 940−5900 nS, respectively. Open conductance values of individual solid-state nanopores were measured by ramping at 0.4 mV/s over ±10 mV. The conductance of the ~25 nm diameter nanopore sample, free of bilayer (Figures 5A and 6), was measured to be 2765 nS, which falls in the reasonable range of conductance values for 20−50 nm nanopores.

Simultaneous AFM and Electrical Recording of a Suspended Lipid Bilayer. Following the deposition of 1,2-diphytanoyl-*sn*-glycero-3-phosphocholine (DiPhyPC) bilayers

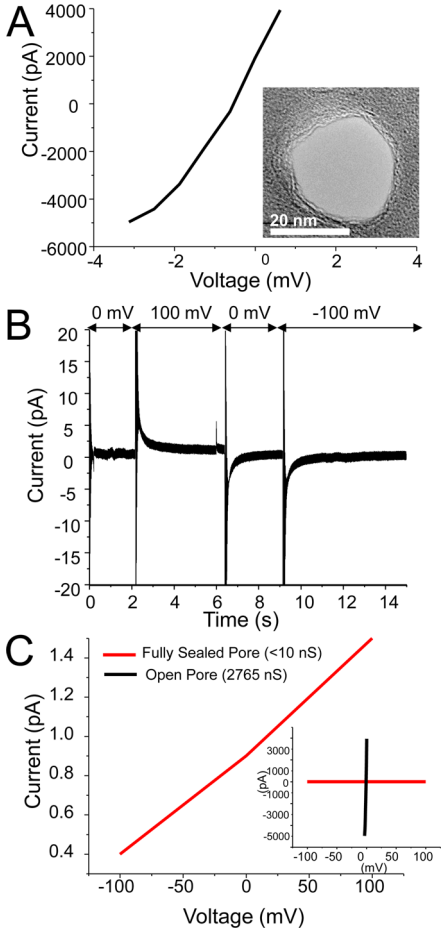

Figure 5. (A) *I*−*V* curve of an open nanopore shown in the inset image measuring ~25 nm with a conductance of 2765 nS. This nanopore was used in the simultaneous AFM imaging and electrophysiology measurements in panels B and C and Figures 6 and 7. Scale bar = 20 nm. (B) Ionic current recording of DiPhyPC lipid bilayer deposited over the nanopore in 1 M KCl electrolyte solution. The observed conductance was <10 pS. (C) *I*−*V* curve of the nanopore from panel A after deposition of a DiPhyPC lipid bilayer. The observed conductance was reduced to <10 pS, indicating a full seal of the nanopore by the bilayer. The inset compares the *I*−*V* curves of the open nanopore (black) and DiPhyPC bilayer-sealed conductance (red).

dx.doi.org/10.1021/am500639q | ACS Appl. Mater. Interfaces 2014, 6, 5290−5296

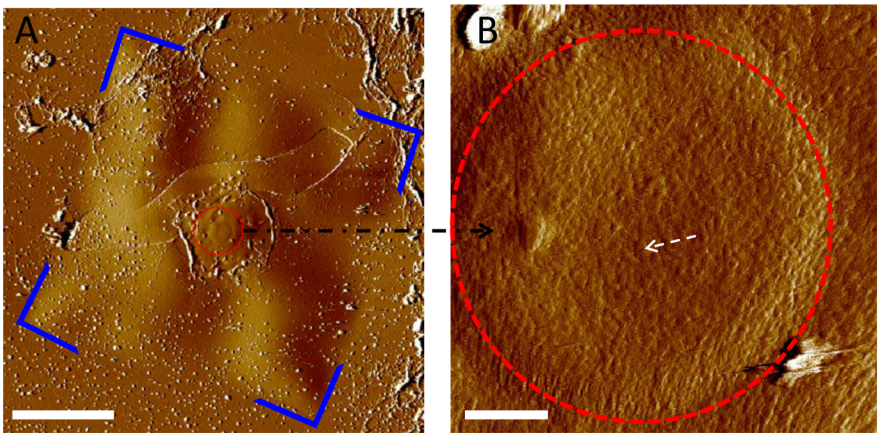

Figure 6. (A) AFM deflection image of 20 × 20 μm^2 area containing the nanopore without a deposited bilayer (outlined in blue). The 1 μm area containing the graphene/Al_2O_3 membrane and a single nanopore are observed in the center of the square. The black arrow shows the zoomed view of this area in panel B. Scale bar = 5 μm. (B) High-resolution AFM image of the 1 μm area containing the graphene/Al_2O_3 membrane and a single nanopore (outlined in red) with no bilayer present. The white arrow indicates the location of the nanopore. Scale bar = 250 nm.

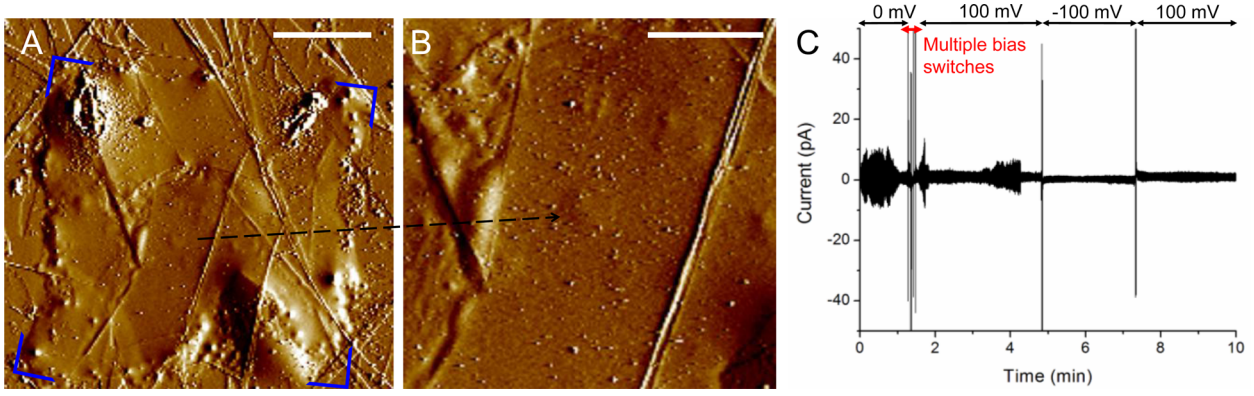

Figure 7. (A) AFM deflection image of square area containing the nanopore after the deposition of the DiPhyPC bilayer (corners highlighted blue) obtained while simultaneously recording ionic conductance. AFM image corresponds to the same area shown in Figure 4A. The 1 μm area containing the graphene/Al_2O_3 membrane and a single nanopore is observed in the center of the square. The black arrow points to the zoomed view of this area in panel B. Scale bar = 5 μm. (B) High-resolution AFM image of the 1 μm area containing the graphene/Al_2O_3 membrane and a single nanopore. Scale bar = 2 μm. (C) Ionic current recording trace obtained while AFM imaging. The initial noise increases at the beginning of the recording and during the 2−4 min time of recording correlate to physical interactions with the system (AFM base and Faraday cage door) and subside upon establishment of physical isolation of the entire system. Applied voltages of ±100 mV were applied to confirm pore sealing.

on the nanopore support mounted in the double-chamber cup system, the pore conductance decreased to <10 pS, as measured in the range ±100 mV (Figure 5C, red). The capacitance of the device with the bilayer was measured to be ~375 pF. Contributing factors to this value may include current passing through the Al_2O_3 layer to the graphene sheet, which increases the capacitive area and the geometry of a thin membrane.[1,40,48] However, capacitances in these ranges are frequently utilized for planar lipid bilayer (PLB) recording of ion channels.[49] In other experiments, partial sealing of the same nanopore was observed by conductance value to drop only to ~0.83 nS (data not shown), indicating an incomplete seal.

The integrity of the fully sealed suspended lipid bilayer, as determined by capacitance and electrical recording, remained stable while engaging the AFM (Figure 7). The interaction force of the AFM was minimized such that it did not interfere with the activity or structure of membrane. The AFM images in Figure 7A,B of the suspended bilayer over the nanopore shows complete coverage. The electrical recording and simultaneously obtained AFM images of the bilayer over the nanopore are shown in Figure 7. Increases in noise were observed during the adjustment of the Faraday cage during the electrical recording. Throughout the AFM imaging (>1 h), switching of the voltage bias did not impact the conductance value of the bilayer.

DISCUSSION

We have developed a nanoscale thin-film support integrated with our newly developed double chamber capable of simultaneous electrical recording and AFM imaging of biological membranes and membrane proteins. The practicality and benefit of this system was demonstrated by structural imaging while measuring the ion-insulating properties of suspended lipid bilayer membranes.

Each step in the fabrication of the nanopore support was chosen with consideration for the ease of fabrication as well as function. A silicon dioxide film on silicon is an ideal material combination to use for the base structure of the nanopore support because of its well-characterized electrical properties, reproducibility, and commercial availability.[32,42,50] Silicon dioxide provides an insulating coating to the large area of the substrate, an essential property to isolate the two compartments of the electrical recording setup. FIB offers a fast and easily

controlled approach for opening the 1 μm hole in the sample to allow for diffusion of electrolytes through the nanopore. Graphene binds tightly to the SiO_2 upon drying, which secures it as a suspended insulating membrane over the FIB gaping hole. In contrast to the multilayer graphene-based structure described by Venkatesan et al., using a single graphene-deposition step allows us to achieve a suspended membrane thickness that is more commensurate with that of a lipid bilayer while still providing good mechanical support.[10] Electrical insulation and structural reinforcement was provided by deposition of 5 nm Al_2O_3 using ALD, which creates a uniform coating with a minimal increase in membrane thickness.[10,31,50] The final graphene/Al_2O_3 membrane surrounding the nanopore is <10 nm. TEM drilling allows positioning the bilayer support on the nanometer scale.[2,42]

Nanopore supports that show a smooth surface in AFM revealed the location and size of the nanopore itself (Figures 4C and 6), and, to our knowledge, AFM images of such small nanopores in graphene/Al_2O_3 membranes have not been previously shown. Characterizing the local environment of a solid-state nanopore by AFM could potentially be used in single-molecule studies by functionalizing the AFM tip. Additionally, the high-resolution AFM imaging of a 20 nm nanopore, as in Figure 4C, suggests membrane proteins in a similar size range may be individually probed in future simultaneous structure−conductance studies.[12,13,23,24] Individual ion channels in supported membranes have often been resolved at larger scan sizes.[12,13,23,24,51−54] These solid-state nanopores are therefore suitable for the intended application of ion channel studies. With this technology, the structure of suspended bilayers or membrane proteins in suspended bilayers may be explored to achieve a better understanding of their function.

Future work with lipid bilayers and the nanopore substrates will investigate the conductance of membrane proteins. The aim of these efforts will be to resolve individual open and closed channel structures localized in the suspended bilayer and to correlate characteristic channel conductances.

CONCLUSIONS

The use of a defined solid-state single-nanopore support in AFM allows for localized characterization in and around the nanopore. We have used this nanopore support to combine both imaging with AFM and functional mapping with bilayer electrical recording. We show that single solid-state nanopores can be fabricated in graphene reinforced with Al_2O_3. The hierarchy of the sample structure allows for quick and easy location of the single nanopore in AFM. This enables accurate identification of a nanoporous thin film, such as lipid bilayers with embedded ion channels, when suspended over this nanopore. The presence of suspended bilayers across the electrical recording path was confirmed and characterized through conductance and capacitance measurements (Figure 5). Small scan sizes, <1 μm, and repeated stable imaging of the suspended bilayers (Figure 7) suggest high-resolution imaging of thin lipid membranes and membrane proteins is possible. Correlated structure and activity information on ion channels obtained using this integrated system will open the door for the study of basic physiological and biological systems as well as for defining the underlying mechanisms of pathophysiology and diseases, including neurodegenerative diseases, drug addiction, biological pathways, and protein structures. The system described here can be applied more broadly to other thin-film-based techniques, including molecular separation, DNA sequencing, and catalysis.

AUTHOR INFORMATION

Corresponding Author

*E-mail: rlal@ucsd.edu.

Author Contributions

⊥These authors contributed equally to this work.

Notes

The authors declare no competing financial interest.

ACKNOWLEDGMENTS

We thank CalIT2 facilities at UCSD Nano3 and UCI Microscopy Center for their excellent technical support. This research was partially funded by NSF-GRF, NDSEG, ARCS Foundation San Diego, and NIDA grants R01DA024871 and R01DA025296 to R.L. and F31DA034562 to B.M.

REFERENCES

(1) Merchant, C. A.; Healy, K.; Wanunu, M.; Ray, V.; Peterman, N.; Bartel, J.; Fischbein, M. D.; Venta, K.; Luo, Z.; Johnson, A. T. C.; et al. DNA Translocation through Graphene Nanopores. *Nano Lett.* **2010**, *10*, 2915−2921.

(2) Chang, H.; Kosari, F.; Andreadakis, G.; Alam, M. A.; Vasmatzis, G.; Bashir, R. DNA-Mediated Fluctuations in Ionic Current through Silicon Oxide Nanopore Channels. *Nano Lett.* **2004**, *4*, 1551−1556.

(3) Wanunu, M.; Sutin, J.; McNally, B.; Chow, A.; Meller, A. DNA Translocation Governed by Interactions with Solid-State Nanopores. *Biophys. J.* **2008**, *95*, 4716−4725.

(4) Wanunu, M.; Meller, A. Chemically Modified Solid-State Nanopores. *Nano Lett.* **2007**, *7*, 1580−1585.

(5) Branton, D.; Deamer, D. W.; Marziali, A.; Bayley, H.; Benner, S. A.; Butler, T.; Di Ventra, M.; Garaj, S.; Hibbs, A.; Huang, X.; et al. The Potential and Challenges of Nanopore Sequencing. *Nat. Biotechnol.* **2008**, *26*, 1146−1153.

(6) Jackson, E. A.; Hillmyer, M. A. Nanoporous Membranes Derived from Block Copolymers: From Drug Delivery to Water Filtration. *ACS Nano* **2010**, *4*, 3548−3553.

(7) O'Regan, B.; Grätzel, M. A Low-cost, High-Efficiency Solar Cell Based on Dye-sensitized Colloidal TiO_2 Films. *Nature* **1991**, *353*, 737−740.

(8) Wang, D.; Zhang, Y.; Wang, J.; Peng, C.; Huang, Q.; Su, S.; Wang, L.; Huang, W.; Fan, C. Template-Free Synthesis of Hematite Photoanodes with Nanostructured ATO Conductive Underlayer for PEC Water Splitting. *ACS Appl. Mater. Interfaces* **2014**, *6*, 36−40.

(9) Sanchez, C.; Boissière, C.; Grosso, D.; Laberty, C.; Nicole, L. Design, Synthesis, and Properties of Inorganic and Hybrid Thin Films Having Periodically Organized Nanoporosity. *Chem. Mater.* **2008**, *20*, 682−737.

(10) Venkatesan, B. M.; Estrada, D.; Banerjee, S.; Jin, X.; Dorgan, V. E.; Bae, M.-H.; Aluru, N. R.; Pop, E.; Bashir, R. Stacked Graphene-Al_2O_3 Nanopore Sensors for Sensitive Detection of DNA and DNA-Protein Complexes. *ACS Nano* **2012**, *6*, 441−450.

(11) Wanunu, M.; Dadosh, T.; Ray, V.; Jin, J.; McReynolds, L.; Drndić, M. Rapid Electronic Detection of Probe-Specific microRNAs Using Thin Nanopore Sensors. *Nat. Nanotechnol.* **2010**, *5*, 807−814.

(12) Lin, H.; Bhatia, R.; Lal, R. Amyloid Beta Protein Forms Ion Channels: Implications for Alzheimer's Disease Pathophysiology. *FASEB J.* **2001**, *15*, 2433−2444.

(13) Quist, A. Amyloid Ion Channels: A Common Structural Link for Protein-Misfolding Disease. *Proc. Natl. Acad. Sci. U.S.A.* **2005**, *102*, 10427−10432.

(14) Dobson, C. M. Protein Folding and Misfolding. *Nature* **2003**, *426*, 884−890.

(15) Ackerman, M. J.; Clapham, D. E. Ion Channels − Basic Science and Clinical Disease. *N. Engl. J. Med.* **1997**, *336*, 1575−1586.

(16) Fotiadis, D.; Scheuring, S.; Müller, S. A.; Engel, A.; Müller, D. J. Imaging and Manipulation of Biological Structures with the AFM. *Micron* **2002**, *33*, 385−397.
(17) Lal, R.; John, S. A. Biological Applications of Atomic Force Microscopy. *Am. J. Physiol.: Cell Physiol.* **1994**, *266*, C1−C21.
(18) Hörber, J. K. H.; Miles, M. J. Scanning Probe Evolution in Biology. *Science* **2003**, *302*, 1002−1005.
(19) Lal, R.; Yu, L. Atomic Force Microscopy of Cloned Nicotinic Acetylcholine Receptor Expressed in Xenopus Oocytes. *Proc. Natl. Acad. Sci. U.S.A.* **1993**, *90*, 7280−7284.
(20) Pelling, A. E.; Li, Y.; Shi, W.; Gimzewski, J. K. Nanoscale Visualization and Characterization of *Myxococcus xanthus* Cells with Atomic Force Microscopy. *Proc. Natl. Acad. Sci. U.S.A.* **2005**, *102*, 6484−6489.
(21) Czajkowsky, D. M.; Iwamoto, H.; Cover, T. L.; Shao, Z. The Vacuolating Toxin from *Helicobacter pylori* Forms Hexameric Pores in Lipid Bilayers at Low pH. *Proc. Natl. Acad. Sci. U.S.A.* **1999**, *96*, 2001−2006.
(22) Fantner, G. E.; Barbero, R. J.; Gray, D. S.; Belcher, A. M. Kinetics of Antimicrobial Peptide Activity Measured on Individual Bacterial Cells Using High-Speed Atomic Force Microscopy. *Nat. Nanotechnol.* **2010**, *5*, 280−285.
(23) Connelly, L.; Jang, H.; Arce, F. T.; Capone, R.; Kotler, S. A.; Ramachandran, S.; Kagan, B. L.; Nussinov, R.; Lal, R. Atomic Force Microscopy and MD Simulations Reveal Pore-Like Structures of All-D-Enantiomer of Alzheimer's β-Amyloid Peptide: Relevance to the Ion Channel Mechanism of AD Pathology. *J. Phys. Chem. B* **2012**, *116*, 1728−1735.
(24) Connelly, L.; Jang, H.; Arce, F. T.; Ramachandran, S.; Kagan, B. L.; Nussinov, R.; Lal, R. Effects of Point Substitutions on the Structure of Toxic Alzheimer's β-amyloid Channels: Atomic Force Microscopy and Molecular Dynamics Simulations. *Biochemistry* **2012**, *51*, 3031−3038.
(25) Lal, R.; Kim, H.; Garavito, R. M.; Arnsdorf, M. F. Imaging of Reconstituted Biological Channels at Molecular Resolution by Atomic Force Microscopy. *Am. J. Physiol.* **1993**, *265*, C851−C856.
(26) Lal, R. Imaging Molecular Structure of Channels and Receptors with an Atomic Force Microscope. *Scanning Microsc., Suppl.* **1996**, *10*, 81−95 discussion 95−96.
(27) Yang, J.; Tamm, L. K.; Tillack, T. W.; Shao, Z. New Approach for Atomic Force Microscopy of Membrane Proteins: The Imaging of Cholera Toxin. *J. Mol. Biol.* **1993**, *229*, 286−290.
(28) Hansma, P. K.; Elings, V. B.; Marti, O.; Bracker, C. E. Scanning Tunneling Microscopy and Atomic Force Microscopy: Application to Biology and Technology. *Science* **1988**, *242*, 209−216.
(29) Lal, R.; Arnsdorf, M. F. Multidimensional Atomic Force Microscopy for Drug Discovery: A Versatile Tool for Defining Targets, Designing Therapeutics and Monitoring Their Efficacy. *Life Sci* **2010**, *86*, 545−562.
(30) Ionescu-Zanetti, C.; Cheung, K.; Lal, R.; Lee, L. P. Simultaneous Imaging of Ionic Conductivity and Morphology of a Microfluidic System. *J. Appl. Phys.* **2003**, *93*, 10134−10136.
(31) Venkatesan, B. M.; Bashir, R. Nanopore Sensors for Nucleic Acid Analysis. *Nat. Nanotechnol.* **2011**, *6*, 615−624.
(32) Quist, A. P.; Chand, A.; Ramachandran, S.; Daraio, C.; Jin, S.; Lal, R. Atomic Force Microscopy Imaging and Electrical Recording of Lipid Bilayers Supported over Microfabricated Silicon Chip Nanopores: Lab-on-a-Chip System for Lipid Membranes and Ion Channels. *Langmuir* **2007**, *23*, 1375−1380.
(33) Wanunu, M. Nanopores: A Journey Towards DNA Sequencing. *Phys. Life Rev.* **2012**, *9*, 125−158.
(34) Bahrami, A.; Doğan, F.; Japrung, D.; Albrecht, T. Solid-State Nanopores for Biosensing with Submolecular Resolution. *Biochem. Soc. Trans.* **2012**, *40*, 624−628.
(35) Iqbal, S. M.; Bashir, R. Nanoelectronic-Based Detection for Biology and Medicine. In *Springer Handbook of Automation*; Springer: New York, 2009; Chapter 81, pp 1433−1449.
(36) Jiang, C.; Markutsya, S.; Pikus, Y.; Tsukruk, V. V. Freely Suspended Nanocomposite Membranes as Highly Sensitive Sensors. *Nat. Mater.* **2004**, *3*, 721−728.
(37) Smeets, R. M. M.; Keyser, U. F.; Krapf, D.; Wu, M.-Y.; Dekker, N. H.; Dekker, C. Salt Dependence of Ion Transport and DNA Translocation through Solid-State Nanopores. *Nano Lett.* **2006**, *6*, 89−95.
(38) Oukhaled, A.; Bacri, L.; Pastoriza-Gallego, M.; Betton, J.-M.; Pelta, J. Sensing Proteins through Nanopores: Fundamental to Applications. *ACS Chem. Biol.* **2012**, *7*, 1935−1949.
(39) Allen, M. J.; Tung, V. C.; Kaner, R. B. Honeycomb Carbon: A Review of Graphene. *Chem. Rev.* **2010**, *110*, 132−145.
(40) Banerjee, S.; Shim, J.; Rivera, J.; Jin, X.; Estrada, D.; Solovyeva, V.; You, X.; Pak, J.; Pop, E.; Aluru, N.; Bashir, R. Electrochemistry at the Edge of a Single Graphene Layer in a Nanopore. *ACS Nano* **2013**, *7*, 834−843.
(41) Wells, D. B.; Belkin, M.; Comer, J.; Aksimentiev, A. Assessing Graphene Nanopores for Sequencing DNA. *Nano Lett.* **2012**, *12*, 4117−4123.
(42) Storm, A. J.; Chen, J. H.; Ling, X. S.; Zandbergen, H. W.; Dekker, C. Fabrication of Solid-State Nanopores with Single-Nanometre Precision. *Nat. Mater.* **2003**, *2*, 537−540.
(43) Ennos, A. E. The Origin of Specimen Contamination in the Electron Microscope. *Br. J. Appl. Phys.* **1953**, *4*, 101.
(44) Kongsuphol, P.; Fang, K. B.; Ding, Z. Lipid Bilayer Technologies in Ion Channel Recordings and Their Potential in Drug Screening Assay. *Sens. Actuators, B* **2013**, *185*, 530−542.
(45) Venkatesan, B. M.; Polans, J.; Comer, J.; Sridhar, S.; Wendell, D.; Aksimentiev, A.; Bashir, R. Lipid Bilayer Coated Al_2O_3 Nanopore Sensors: Towards a Hybrid Biological Solid-State Nanopore. *Biomed. Microdevices* **2011**, *13*, 671−682.
(46) Garaj, S.; Hubbard, W.; Reina, A.; Kong, J.; Branton, D.; Golovchenko, J. A. Graphene as a Subnanometre Trans-Electrode Membrane. *Nature* **2010**, *467*, 190−193.
(47) Meckes, B.; Teran Arce, F.; Connelly, L. S.; Lal, R. Insulated Conducting Cantilevered Nanotips and Two-Chamber AFM for High Resolution Ion Sensing AFM. *Sci. Rep.*10.1038/srep04454.
(48) Venta, K.; Shemer, G.; Puster, M.; Rodríguez-Manzo, J. A.; Balan, A.; Rosenstein, J. K.; Shepard, K.; Drndić, M. Differentiation of Short, Single-Stranded DNA Homopolymers in Solid-State Nanopores. *ACS Nano* **2013**, *7*, 4629−4636.
(49) Wonderlin, W. F.; Finkel, A.; French, R. J. Optimizing Planar Lipid Bilayer Single-Channel Recordings for High Resolution with Rapid Voltage Steps. *Biophys. J.* **1990**, *58*, 289−297.
(50) Storm, A. J.; Chen, J. H.; Ling, X. S.; Zandbergen, H. W.; Dekker, C. Electron-Beam-Induced Deformations of SiO_2 Nanostructures. *J. Appl. Phys.* **2005**, *98*, 014307-1−014307-8.
(51) Yeager, M.; Harris, A. L. Gap Junction Channel Structure in the Early 21st Century: Facts and Fantasies. *Curr. Opin. Cell Biol.* **2007**, *19*, 521−528.
(52) Ambrosi, C.; Boassa, D.; Pranskevich, J.; Smock, A.; Oshima, A.; Xu, J.; Nicholson, B. J.; Sosinsky, G. E. Analysis of Four Connexin26 Mutant Gap Junctions and Hemichannels Reveals Variations in Hexamer Stability. *Biophys. J.* **2010**, *98*, 1809−1819.
(53) Studer, A.; Han, X.; Winkler, F. K.; Tiefenauer, L. X. Formation of Individual Protein Channels in Lipid Bilayers Suspended in Nanopores. *Colloids Surf., B* **2009**, *73*, 325−331.
(54) Tokumasu, F.; Jin, A. J.; Dvorak, J. A. Lipid Membrane Phase Behaviour Elucidated in Real Time by Controlled Environment Atomic Force Microscopy. *J. Electron Microsc.* **2002**, *51*, 1−9.